Hindawi
Shock and Vibration
Volume 2021, Article ID 4593221, 9 pages
https://doi.org/10.1155/2021/4593221

Research Article

Numerical Simulation on Selection of Optimal Delay Time for Precise Delay Blasting

Jun Ma,[1] **Xianglong Li**,[1,2] **Jianguo Wang**,[1,2] **Qiang Li**,[1] **Ting Zuo**,[1] **Xiao Wu**,[3] **and Meng Hou**[3]

[1]*Faculty of Land and Resources Engineering of Land and Resources Engineering, Kunming University of Science and Technology, Kunming 650093, Yunnan, China*
[2]*Yunnan Key Laboratory of Sino-German Blue Mining and Utilization of Special Underground Space, Kunming University of Science and Technology, Kunming 650093, Yunnan, China*
[3]*Zhejiang Gaoneng Corporation of Blasting Engineering Co., Ltd., Hangzhou 310012, Zhejiang, China*

Correspondence should be addressed to Jianguo Wang; wangjg0831@163.com

Received 23 June 2021; Revised 6 August 2021; Accepted 18 August 2021; Published 13 September 2021

Academic Editor: Jun Wang

In the traditional presplitting blasting, the presplit holes are generally uniformly initiated, which causes local damage to the retained rock mass while forming the damping ditch. In order to determine the optimal delay time of the precise delay initiation hole by hole, the finite element software ANSYS/LS-DYNA is used to build a blasting model of the concrete, which includes concrete, explosive, and air to simulate the crack forming process of the presplitting hole under various initiation modes. Four kinds of initiation modes for blasting, namely, simultaneous initiation with 0 ms, 9 ms, 12 ms, and 15 ms of delay between adjacent holes, are set up to determine the exact delay time of the best presplitting effect. The simulation results show that when the prehole detonates simultaneously, the inner hole crack penetrates the fastest, but the peak stress around the hole is up to 147.9 MPa. When interhole delayed initiation is used, although the time of interhole crack penetration is prolonged, the stress coupling is generated around the precrack and the maximum stress is obviously reduced. The maximum stress generated under the three delayed initiation conditions is only 76.8 MPa. Considering the requirement of damage control of surrounding rock mass and the rapid formation of precrack, 9 ms delay time is determined as the precise delay time of this test.

1. Introduction

When presplitting blasting is used in the engineering practice, it is important to form satisfying precracks of the presplit holes and minimize the damage on the surrounding rock by blasting. Traditionally, the presplitting blasting mainly adopts the simultaneous initiation method, and the explosion stress waves superimpose onto each other during the joint formation process, which causes great damage to the surrounding rock. It is generally believed that the precrack is formed due to the combined action of the explosion shock wave and the explosion gas, and the strain wave also makes a contribution to the crack development process [1]. Liu et al. [2, 3] studied the crack propagation from two aspects, namely, the charge amount and charge mode, and found that the mechanical characteristics of the primary cracks and the secondary cracks are similar when the same charge amount is adopted. Through analysis by LS-DYNA, Qu and Liu [4] found the joint effect is the best when the joints are perpendicular to the connection line of the blast holes. Besides, some researchers studied the mechanism and propagation regularity of the precrack cracking through other methods and influencing factors [5–7], and the results show that when the presplitting blasting is implemented, the simultaneous blasting exhibits the best cracking effect, but the construction environment is very complex which requires controlled presplitting. According to the maximum single-shot charge of the split blasting, segmented initiation of the presplit holes is required, which reduces the blasting vibration and has no influence on the effect of the presplitting blasting at the same time. Yu et al. [8, 9] used numerical simulation software to simulate the blasting

situation of double hole under various ground stress conditions and joint angle and obtained the influence of these two factors on the expansion of blasting lines. Wang and Chen [10] used numerical methods to study the influence of charge structures on surrounding rock damage caused by blasting; the numerical simulation results show that the charging structure of water and slotted pipe can achieve a good blasting effect and reduce the damage of surrounding rock. Guo et al. [11] used finite element software ANASYS and LS-DYNA to analyze the effect of coal mass on cracking under shaped energy blasting, and the expansion mechanism was studied through this numerical model. In the work of Gao and Lei [12], finite element software was used to simulate the cutting and excavation process and analyze the stress field and domino effects (such as von Mises) in the rock during the millisecond delay blasting process, along with the propagation regularity of the particle vibration velocity. In addition, numerical software can also be applied to simulate the tunnel excavation in the blasting tests and the crack propagation under blasting load [13–15].

However, there are too many influencing factors in minefield tests and model tests that could not be accurately analyzed singly through the tests. In comparison, this problem can be solved by numerical simulation analysis methods which can set various model parameters and experimental conditions. The research needs for a single factor can be achieved by combining the results of the field tests and model tests, thus obtaining comprehensive and accurate analysis results for specific research purposes. In recent years, the application of digital electronic detonators makes the research on precise time-delay controlled blasting technology a hot spot. In the past, presplitting blasting was usually blasted at the same time due to its characteristics, but the damage on surrounding rock is more serious when it is blasted at the same time, so the time-delay controlled blasting technology is proposed. The application of the controlled blasting technology of presplit blasting is a breakthrough technology. This paper intends to use the finite element software ANSYS/LS-DYNA to study the cracking mechanism of hole-by-hole presplitting blasting and the effect of delay time on the cracking mechanism and then to determine the optimal delay time.

2. Numerical Simulation Process

2.1. Parameters Setting of the Numerical Model. The concrete model test by Wu et al. [16] is based on the similarity theorem, and in this test, the effect of hole spacing and the noncoupling coefficient on the precrack width and half hole rate was analyzed. It was found that when the noncoupling coefficient is 2.16 and the hole spacing is 8 times of the aperture, the effect of crack formation and protection of surrounding rock is the best. According to this model test, the parameters such as noncoupling coefficient, blast hole diameter, hole distance, explosive type, and required charge amount were determined through numerical simulations. The actual pouring model picture is shown in Figure 1, where the hole distance is 104 mm and the hole diameter is 13 mm. The influence of related parameters on the blasting is studied. The size of the numerical model is 700 mm × 600 mm × 5 mm, and the hole diameter is 13 mm, while the diameter of the cartridge is 6 mm. Besides, the hole distance is set as 104 mm and the explosive parameter in the calculation model is set as hexogen.

Figure 1: The model cast by Wu Xiao.

2.2. Establishment of the Numerical Model. The numerical model takes the model test as the prototype, which consists of three components: air, explosives, and concrete. Referring to the literature [17], keywords are used to define concrete and explosives, and the JWL equation of state is used to describe the relevant parameters of the explosives, as shown in the following equation:

$$P = A\left(1 - \frac{\omega}{R_1 V}\right)e^{(-R_1 V)} + B\left(1 - \frac{\omega}{R_2 V}\right)e^{(-R_2 V)} + \frac{\omega E_0}{V}, \tag{1}$$

where V is the relative specific volume of the detonation product of dimensionless; E_0 is the initial internal energy of the explosive per unit volume (Pa); ρ is the explosive density (g/cm^3); D is the detonation velocity (m/s); P is the explosion pressure (kPa); and A, B, R_1, R_2, and ω are all parameters related to explosive materials. The simulated explosive is set to hexogen, and the core diameter is about 6 mm. The corresponding model parameters are shown in Table 1.

During the explosion process, the loading strain rate of the explosive medium, i.e., concrete, increases as the burst center distance of the media decreases, the maximum value of which can reach 104 s^{-1}. The material keyword ∗MAT_JOHNSON_HOLMGUIST_CONCRETE is used to define the concrete medium. When the strain rate increases, the dynamic compressive strength of the concrete also increases, with the concrete material deforming at the same time.

Equation (2) is used to express the strength of the HJC material model [18, 19]:

$$\sigma * = \left[A(1 - D) + BP^{*N}\right]\left(1 + C\ln\varepsilon^{*}\right). \tag{2}$$

In the formula, $\sigma^* = \sigma / f_c$ is the ratio of the actual equivalent stress to the static yield strength, where σ is the

Table 1: Main parameters of the material model of hexogen explosive.

Parameter	ρ (g/cm^3)	D (m/s)	P (GPa)	A	B	R_1	R_2	ω	E_o (GJ·m^{-3})
Value	1.5	7000	23.1	611.3	10.65	4.4	1.2	0.32	8.13

actual equivalent stress and f_c is the quasistatic uniaxial compressive strength; $P^* = P/f_c$ is the dimensionless pressure, where p is the actual hydrostatic pressure of the unit; $\varepsilon^* = \varepsilon/\varepsilon_0$ is the dimensionless strain rate, where $\dot{\varepsilon}$ is the true strain rate and $\dot{\varepsilon}_0$ is the reference strain rate; A is the normalized viscous strength; B is the normalized pressure hardening coefficient; C is the strain rate influence coefficient; N is the normalized pressure hardening index; D is the damage factor; and $S_{\max}$ is the maximum value that the normalized equivalent stress can reach.

The calculation of damage factor D $(0 \le D \le 1)$ is shown in equations (3) and (4):

$$D = \sum \frac{\Delta\varepsilon_p + \Delta U_p}{\varepsilon_p^f + \mu_p^f}, \tag{3}$$

$$f(p) = \varepsilon_p^f + \mu_p^f = D_1 \left(p^* + T^*\right)^{D_2}, \tag{4}$$

where $\Delta\varepsilon_p$ is the increment of the equivalent plastic strain, $\Delta\mu_p$ is the increment of the equivalent volumetric strain, $f(p)$ is the plastic strain when the material breaks under normal pressure p, p^* is the normalized pressure, T^* is the maximum tensile static pressure which the material can withstand, and D_1 and D_2 are damage constants.

The HJC model uses a segmented equation of state to describe the relationship between the static water pressure and volume strain of concrete and uses different polynomial equations to describe the relationship between the static water pressure and volume strain in the elastic zone, the crushing zone, and the compaction zone in the concrete compression process.

In the elastic zone $(0 < \mu \le \mu_{\text{crush}})$,

$$P = K\mu, \tag{5}$$

where P is the hydrostatic pressure of the element, K is the elastic modulus of the concrete element, and μ is the volume strain of the element.

In the crushing area $(\mu_{\text{crush}} < \mu \le \mu_{\text{lock}})$,

$$P = P_{\text{crush}} + K_{\text{lock}} \left(\mu - \mu_{\text{crush}}\right), \tag{6}$$

where P_{crush} is the hydrostatic pressure in the unit corresponding; $K_{\text{lock}} = (P_{\text{lock}} - P_{\text{crush}})/(\mu_{\text{lock}} - \mu_{\text{crush}})$, where μ_{crush} is the volume strain at the crush point, P_{lock} is the hydrostatic pressure in the unit corresponding to μ_{lock}, and μ_{lock} is the volume strain at compaction point.

In the compaction zone $(\mu \ge \mu_{\text{lock}})$,

$$P = K_1\overline{\mu} + K_2\overline{\mu}^2 + K_3\overline{\mu}^3. \tag{7}$$

In the formula, $\overline{\mu} = (\mu - \mu_{\text{lock}})/(1 + \mu_{\text{lock}})$ is the corrected volume strain and K_1, K_2, and K_3 are the material constants of concrete.

Table 2 shows the main parameters of the HJC concrete constitutive model. Among them, G, F_C, P_C, and T are the mechanical test results. The remaining parameters are derived from the test with large strain, high strain rate, and high pressure of reference [20].

The model is divided into a mapped grid, and the number of grid cells is 46104. A nonreflective boundary constraint is applied on the top and bottom of the model with a total of 4 parts of concrete, air, explosive 1, and explosive 2. The maximum compressive strength of the C30 concrete around the blast hole, i.e., 29.96 MPa, is taken as the failure value of the element under dynamic load, and the crack propagation is described by element failure. The model mesh is shown in Figure 2. Four sets of delay times of 0, 9, 12, and 15 ms are carried out through comparison experiments by the numerical model. The unit used for numerical model calculation is cm-g-μs.

3. Simulation Results and Analysis

Before running the LS-DYNA 3D program, five elements are designated as observation points to facilitate analyzing and processing the numerical results [21–40]. As shown in Figure 3, points H69786, H68778, H68787, H62503, and H61486 are selected at the lower part of the centerline of two blast holes, which are signed as A, B, C, D, and E, respectively. The left blast hole is defined as the No. 1 blast hole, and the right one is No. 2. The unit of the distance between elements is mm. After the calculation is completed, the blasting process is described intuitively and detailedly through stress cloud charts and stress curves in time.

3.1. Stress Cloud Charts. The stress cloud of simultaneous initiation of prehole and interhole delay time of 12 ms was taken as an example to describe and analyze. In the stress cloud charts, the stress value of different areas is distinguished by colour.

(1) Simultaneous initiation stress cloud analysis: Figure 4 shows the stress cloud of simultaneous initiation of the presplitting blast hole. It can be seen from Figure 4 that the detonation wave propagates outward in a circular shape in the homogeneous material. At the time of 9 μs after the numerical simulation initiation, the crushing zone and fracturing zone are formed around the hole wall. At the time of 14 μs, the stress waves generated by the two blast holes are gradually superimposed together, forming a stress concentration zone between the two blast holes. The explosion stress waves of the two blast holes have a promoting effect on each other; thus, the cracks are produced between the two blast holes. The hole is connected to the centerline; the colour of the stress superimposed area changes to red

Table 2: Parameters of the HJC constitutive model of concrete.

Item name	Value	Item name	Value
Density $\rho_o/(g{\cdot}cm^{-3})$	2.300	Reference strain rate EPSO	1.000
Shear modulus G/Pa	9.681	Minimum plastic strain EFMIN	0.010
Strength parameter 1 A	0.300	Strength parameter 5 SFMAX	7.000
Strength parameter 2 B	1.730	Volume pressure during crushing $PC/10^{11}$ Pa	$8.000E-05$
Strength parameter 3 C	0.005	Volume strain during crushing UC	$6.200E-04$
Strength parameter 4 N	0.790	Ultimate volume stress $PL/10^{11}$ Pa	$3.470E-02$
Static yield strength $F_c/10^{11}$ Pa	$2.400E-04$	Limit volume strain UL	$8.696E-02$
Tensile strength $T/10^{11}$ Pa	3.037E-05	Damage constant 1 D_1	0.04
Damage constant 2 D_2	1.0	Pressure parameter 2 K_2	−2.430
Pressure parameter 1 K_1	1.160	Pressure parameter 3 K_3	5.06

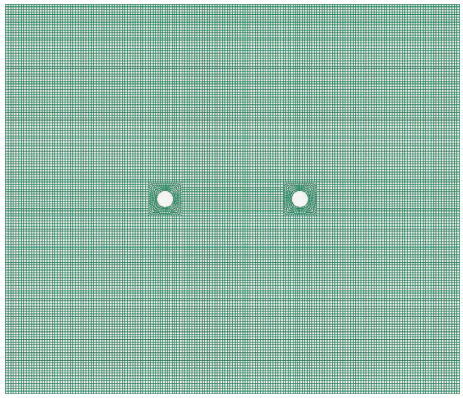

Figure 2: The partition of model mesh.

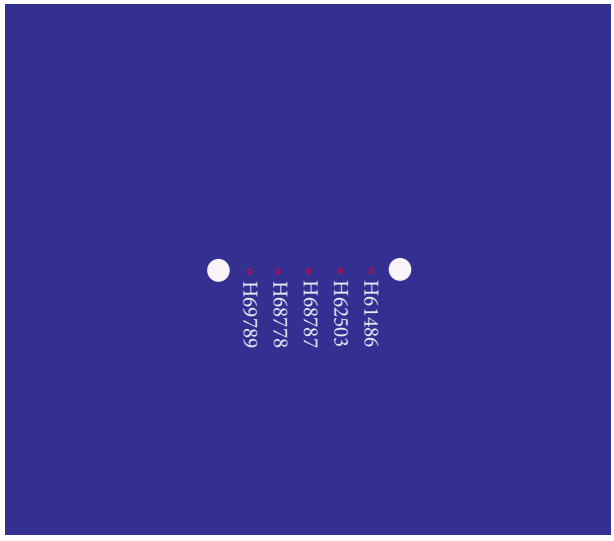

Figure 3: Location of the observation points in the present model.

at 17 μs, which means that the stress in this area rises and reaches the highest of 147.6 MPa. After that, the cracks penetrate at 19 μs, and there is still a high-stress zone around the holes. At 39 μs, the stress wave diffuses to the empty surface of the concrete medium, the reflected tensile stress wave begins to act, the stress concentration phenomenon begins to dissipate, and a "calabash" unloading wave is gradually formed.

(2) Analyze the stress cloud chart of the case with a 12 ms delay time. The stress cloud chart of the batch with 12 ms delayed time is shown in Figure 5. It can be seen from Figure 5 that, after 0.1 ms of the detonation of No. 1 blast hole, the stress wave breaks the blast hole wall and surrounding rock and the detonation stress wave propagates to the entire homogeneous material. A high-stress area appears at the left side of the No. 1 blast hole. When the stress wave reaches the material boundary, a reflected tensile wave is generated, inducing the material boundary stress slightly greater than that of the surrounding. At 9 ms after the explosion, the detonation stress wave of the No. 1 blast hole gradually dissipates on the right side of the homogeneous material and the right side of the No. 2 blast hole remains crushed. The stress around the No. 1 blast hole is about 43.6 MPa. At 12 ms of blasting, the stress generated by the explosion of the No. 1 blast hole gradually dissipates in the entire homogeneous material. At this time, the No. 2 blast hole is detonated, causing the wall of No. 2 blast hole to break. At 12.1 ms, the stress wave generated by the explosion of the No. 2 hole has diffused on the surface of the material. At 12.3 ms, the stress around the No. 2 blast hole was concentrated, the maximum stress is about 56.6 MPa, and the crack between the two holes is completely connected, forming precrack.

Table 3 lists the crack penetration time and the maximum stress around the blast holes under the four delay times. It can be seen from Table 3 that although the fastest crack penetration occurs in the simultaneous blasting, the stress value generated around the blast hole with the delayed detonation is significantly less than that of the simultaneous blasting. Under the four delay times, the smallest stress around the blast hole appears at the case of 15 ms delay with a value of 49.1 MPa and the fastest crack penetration is found at the case of 9 ms delay with a maximum stress value of only 50.7 MPa. In this situation, the damage to the surrounding rock is greatly reduced and the crack can be penetrated as soon as possible.

3.2. Analysis of Effective Stress Curve. The destruction effect of explosives is analyzed by intercepting the von Mises equivalent stress of the model element. von Mises is a yield

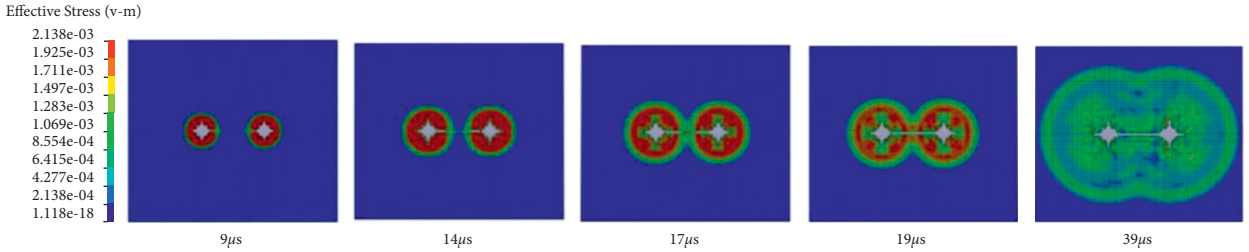

Figure 4: Stress cloud charts of explosive detonation propagation with time.

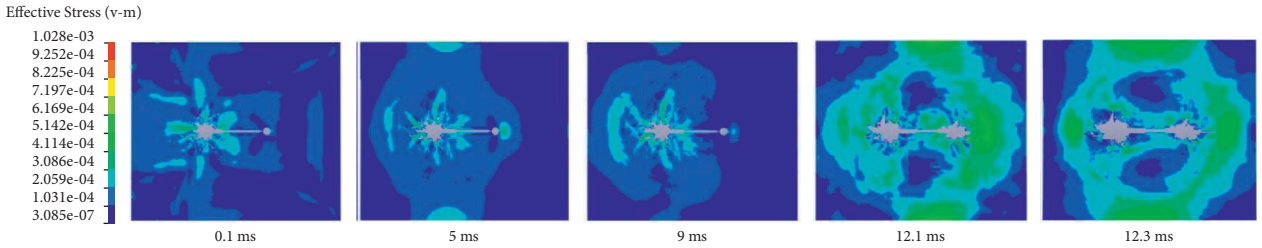

Figure 5: Stress cloud chart of explosive detonation propagation in the case with 12 ms delayed time.

Table 3: Comparison of parameters under four kinds of delay time.

Interhole delay time (ms)	Crack penetration time (μs)	Maximum stress (MPa)
0	19	147.6
9	10.3×10^3	50.7
12	13×10^3	56.6
15	17×10^3	49.1

criterion that describes the stress state by constructing stress contours, and the value of the yield criterion is usually called the equivalent stress. The effective stress curve of each delayed initiation is shown in Figure 6. Combining Figures 4 and 6(a), it can be seen that when the blast holes are all detonated, the stress wave on the homogeneous material starts to spread out from the blast hole. Therefore, the peak stresses of element *A* and element *E* appear first, with the values of 138.8 MPa and 147.6 MPa, respectively. The stress waves of elements *B* and *D* intersect and superpose the stress wave of element *C*, resulting in the effective stress of element *C* being higher than elements *B* and *D*. After the stress wave is transmitted away, the effective stress of each element is greatly reduced.

It can be seen from Figure 6(b) that, in the case with the delayed detonation of 9 ms, the stress wave is in a spherical shape when transmitting to No. 2 blast hole after the detonation of No. 1 blast hole. The peak stress first occurs in element A with a value of 42.6 MPa, followed by elements *B*, *C*, *D*, and *E*, with values of 39.7, 35.3, 20.9, and 13.0 MPa, respectively. The second blast hole detonates at 9 ms after the detonation of the first blast hole, and the produced stress wave transmits to the first blast hole, causing the effective stress of elements to increase successively. The new peak stress appears at element *E* first with a value of 50.7 MPa, followed by elements *D*, *C*, *B*, and *A*, with the stress values of 37.5, 34.0, 32.1, and 30.3 MPa, respectively. After that, the stress wave gradually dissipates and the effective stress curve decreases to zero. This is because at the initiation of the No. 2 blast hole, the explosion stress wave of the No. 1 blast hole has not dissipated yet and the stress superposition is formed between the two holes, resulting in a secondary loading phenomenon. Here, the stress superposition is quantitatively described by the coupling degree of stress waves which is defined as the percentage of the overlap value to the first peak stress value when waves propagate. In this study, the coupling degree of the stress wave is calculated to be 51.69% in the case of a 9 ms delay.

Combining Figure 5 with Figure 6(c), in the case with 12 ms delayed detonation, the stress wave spreads into surrounding homogeneous material after the detonation of No. 1 blast hole and reaches the peak stress within 0.1 ms. At this time, the maximum stress appears in element A with a value of 54.3 MPa and the peak stresses of elements *B*, *C*, *D*, and *E* are 39.5, 36.1, 21.0, and 18.6 MPa, respectively. Before the time reaching 12 ms, the stress value received by each element is relatively stable, which is due to the reason that the stress wave generated by the explosion of the No. 1 blast hole is gradually spreading to the boundary without other interferences. At 12 ms, the No. 2 blast hole detonates and the maximum stresses at elements *E*, *D*, C, *B*, and *A* are 57.3, 45.6, 42.3, 34.9, and 31.8 MPa, respectively, due to the superposition of stresses. The stress quickly drops to about 10 MPa within 0.4 ms, and the coupling degree of stress wave is 67.54%.

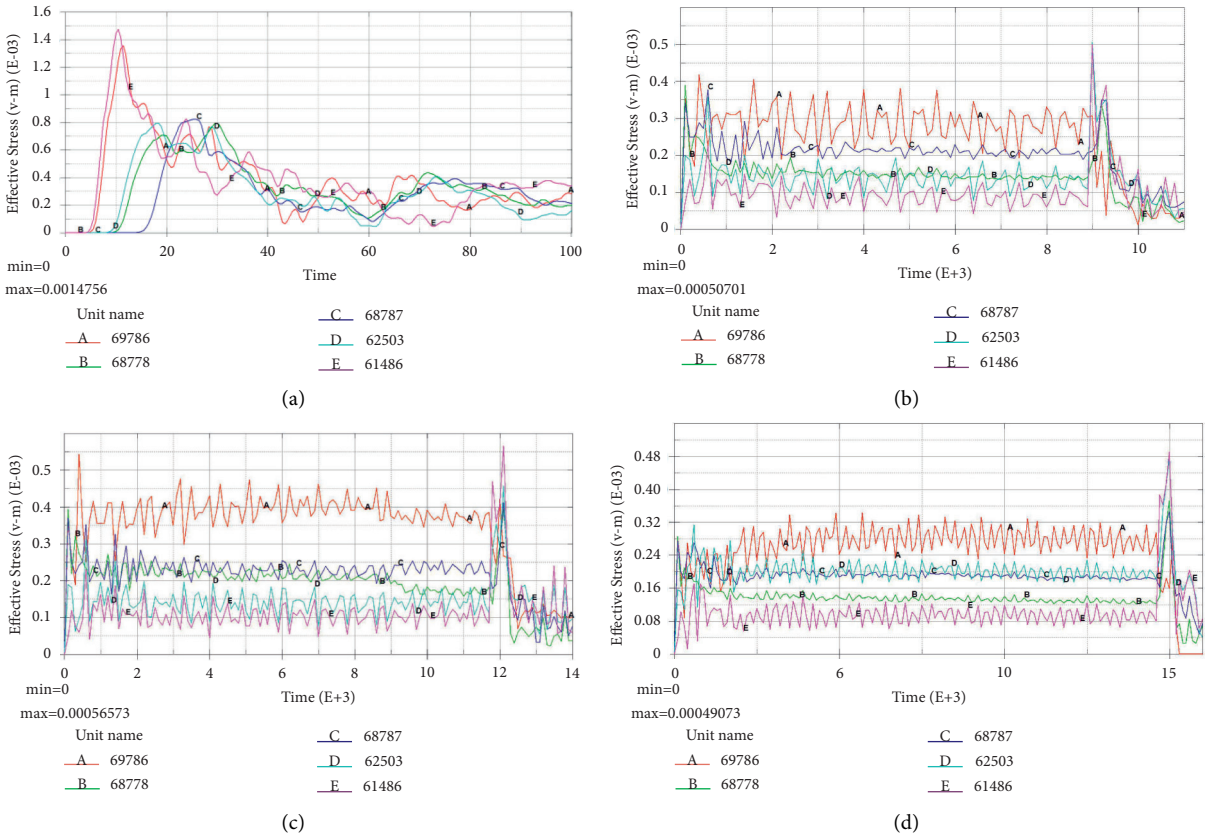

Figure 6: Effective stress curves for each case of delay time. (a) The effective stress curve under simultaneous initiation. The effective stress curve of delayed initiation at (b) 9 ms, (c) 12 ms, and (d) 15 ms.

It can be seen from Figure 6(d) that, under the condition of delayed detonation of 15 ms, the stress of five elements in the homogeneous material surrounding to the No. 1 blast hole increases rapidly after the detonation of No. 1 blast hole. At 0.2 ms after the explosion, the elements *A*, *B*, *C*, and *E* reach stress values of 26.2, 28.3, 27.0, and 22.3 MPa, respectively, and the peak stress appears at element *D* with a value of 31.8 MPa. From 2 ms, the stress fluctuations received by these five elements tend to be balanced with no large changes. It is because the stress wave generated by the detonation of the No. 1 blast hole gradually dissipates from the right side. At 15 ms, the stress received by the detonation elements of the No. 2 blast hole suddenly increases, but the stress superposition is not obvious because the stress due to the blast of the No. 1 blast hole has dissipated. The maximum stress appears at element *E* at 15 ms with a value of 49.1 MPa, and its coupling degree of stress wave is 54.03%. As the homogeneous material begins to shatter and break, the stress received by each element dissipates and decreases to zero quickly.

3.3. Analysis and Discussion of Simulation Results. Numerical simulations are carried out on the above four situations with various delay times, namely, the aligned detonation and detonations with 9 ms, 12 ms, and 15 ms delay time. The analysis and discussion of the simulation results are as follows:

(1) When both holes are detonated simultaneously, the maximum stress value received by element *E* is only 147.6 MPa, while the maximum stress is only 56.6 MPa when the detonation is delayed, with the peak stress of each element reduced by 61.65% compared to the simultaneous detonation. The maximum stress value received by the surrounding rock during the delayed detonation is reduced by 61.65% compared with the maximum stress value received when the holes are detonated simultaneously, which effectively reduces the damage on the surrounding rock. In the case of delay time, the maximum stress is generated after the explosion of the No. 2 blast hole. Because the stress wave generated by the detonation of No. 2 blast hole overlaps with the undissipated stress wave of No. 1 blast hole, the maximum stress is generated after the explosion of No. 2 blast hole, which is later detonated. Therefore, a reasonable delay time can effectively control the damage to the surrounding rock mass.

(2) When the delay time is set, the two peak stresses of the case with 9 ms delay time detonation are 42.6 MPa and 50.7 MPa, respectively, and those for the 12 ms delay time detonation are 54.3 MPa and 57.3 MPa, respectively, while those of the case with 15 ms delay time is 31.8 MPa and 49.1 MPa, respectively. Therefore, the peak stress of the case with 12 ms delay is the largest,

and that of the 15 ms delay case is the smallest, indicating that the case with 12 ms delay time has the greatest damage on the surrounding rock and the case with 15 ms delay is the smallest. The crack penetration time is 9.1, 12.1, and 15.1 ms, respectively, for the cases with 9, 12, and 15 ms delay time. This result indicates that the case with 9 ms delay time forms precrack faster.

(3) The two stress peaks received by element E are compared and analyzed. The coupling degrees of stress wave for the cases with 9 ms, 12 ms, and 15 ms delay time are 51.69%, 67.54%, and 54.03%, respectively, so the case with 12 ms delay time has the most coupling degree with higher energy utilization rate and less energy loss. The case with a 9 ms delay has the fastest precrack formatting speed and causes less damage on the surrounding rock but wastes a certain amount of energy. The case with 12 ms delay time forms the precracks in a higher speed, with the highest energy utilization rate but greater damage on the surrounding rock mass, while the 15 ms delay time case has the slowest speed of formation of precracks and the least damage on the surrounding rock and a certain amount of energy will also be wasted. In summary, according to the requirements for reducing damage on the surrounding rock and rapid formation of precracks, the 9 ms delay is more in line with the purpose of the test than other delay times.

(4) The stress cloud chart and stress curve are used to analyze the delayed initiation and precracking processes, and it is found that when No. 1 blast hole is detonated, a large number of cracks are generated around the blast hole, and the stress is generated throughout the material quickly. The cracks induced by the explosions of the No. 1 and No. 2 blast holes develop along the connecting centerline of the two holes due to the guiding effect. The cracks develop gradually as the stress dissipates, but the crushing zone of the No. 2 blast hole still has large stress and generates small cracks. After the detonations, a large number of cracks are generated around the blast hole and develop along the blast hole connecting the centerline. At the same time, the growth rate of the crack generated by the explosion of the No. 1 blast hole on the blast hole connecting centerline accelerates again until it overlaps the precrack produced by the No. 2 blast hole.

4. Conclusions

Based on the numerical simulation blasting model of concrete, the simulation was carried out on the four situations of the simultaneous initiation of two gun holes and the delayed initiation of 9 ms, 12 ms, and 15 ms between the holes, and the research results were as follows:

(1) Two holes were detonated at the same time, and the cracks between the holes penetrated at $t = 19\ \mu s$. The maximum stress on both sides of the hole reached 147.6 MPa in the process of forming the cracks, which was greater than the stress generated by the three kinds of hole-by-hole initiation set in the numerical model test, and the maximum damage to the surrounding rock was caused.

(2) When the interhole delay time is 9 ms, the crack penetrates at $t = 9.1$ ms, the coupling degree of stress wave is 51.69%, and the peak stress on both sides of the hole is 50.7 MPa, which is reduced by 65.72% compared with simultaneous initiation, and the damage to the surrounding rock mass is obviously weakened.

(3) When the interhole delay time is 12 ms, the crack penetrates at $t = 12.1$ ms, the coupling degree of stress wave is 67.54%, and the peak stress on both sides of the hole is 56.6 MPa, which is 61.65% lower than that of simultaneous initiation.

(4) When the interhole delay time is 15 ms, the crack penetrates at $t = 15.1$ ms, the coupling degree of stress wave is 54.03%, and the peak stress on both sides of the hole is 49.1 MPa, which is 66.73% lower than that of simultaneous initiation.

(5) Taking into account the damage control of surrounding rock mass, energy utilization rate, and precrack penetration rate of blasting load, it is determined that 9 ms delay time is the best accurate delay time between holes of precrack initiation in this numerical test. This method is of guiding significance to the future research of precrack formation and the choice of delay time of precrack blasting by hole.

Data Availability

The data used to support the findings of this study are included within the article.

Disclosure

Xianglong Li is the co-first author.

Conflicts of Interest

The authors declare that they have no conflicts of interest.

Authors' Contributions

Conceptualisation, methodology, validation, data curation, visualisation, and original draft preparation were performed by J. W. and J. M.; data analysis and model parameter determination were performed by X. L.; numerical simulation calculation was done by J. M. and Q. L.; and formal analysis and writing, review, and editing were performed by all authors. The adjustment of the later parameters is completed by T. Z., and the parameter confirmation is completed by X. W. and M. H. All authors have read and agreed to the published version of the manuscript.

Acknowledgments

This study was financially supported by the National Natural Science Foundation of China (No. 51934003), and this support is gratefully appreciated.

References

[1] Y. Xu, Y. P. Meng, and Q. Zong, "Study on range of cranny and length of fissure expansion in fault zone," *Rock and Soil Mechanics*, vol. 1, pp. 81–84, 2002.

[2] J. Liu, Z. Liu, K. Gao, J. Xue, and Y. Lou, "Experimental study of extension characters of cracks in coal seam under blasting load with different charging modes," *Chinese Journal of Rock Mechanics and Engineering*, vol. 35, no. 4, pp. 735–742, 2016.

[3] L. I. Qing, Y. U. Qiang, G. Zhu, G. Wei, and X. U. Shuncheng, "Experimental study of crack propagation under two-hole slotted cartridge blasting with different amounts of charge," *Chinese Journal of Rock Mechanics & Engineering*, vol. 36, no. 9, pp. 2205–2212, 2017.

[4] S. J. Qu and J. F. Liu, "Numerical analysis of joint angle effect on cracking with presplit blasting," *Yantu Lixue/Rock and Soil Mechanics*, vol. 36, no. 1, pp. 189–194-204, 2015.

[5] R. Yang and S. U. Hong, "Experimental study on crack propagation with pre-crack under explosion load," *Journal of China Coal Society*, vol. 44, no. 2, pp. 482–489, 2019.

[6] S. Jhon, L. Li, and J. M. Gernand, "Reliability analysis for mine blast performance based on delay type and firing time," *International Journal of Mining Science & Technology*, vol. 28, no. 2, pp. 46–55, 2018.

[7] H. Tang, K. S. Liang, and Q.F. You, "Discussion on mechanism and effect factors of cracks resulted from pre-splitting blasting," *Blasting*, vol. 27, no. 3, pp. 41–44, 2010.

[8] B. Yu, W. Zhu, C. Wei, and J. Wei, "Numerical simulation on two-hole blasting under different in-situ stress conditions," *Yantu Lixue/Rock and Soil Mechanics*, vol. 34, no. S1, pp. 466–471, 2013.

[9] C. Wei, W. Zhu, Y. Bai, and S. Li, "Numerical simulation on two-hole blasting of rock under different joint angles and in-situ stress conditions," *Lixue Xuebao/Chinese Journal of Theoretical and Applied Mechanics*, vol. 48, no. 4, pp. 926–935, 2016.

[10] X.S. Wang and F.D. Cheng, "Research on surrounding rock damage control blasting by numerical simulation method," *Transactions of Beijing Institute of Technology*, vol. 34, no. 10, pp. 991–996, 2014.

[11] D. Y. Guo, P. F. Lv, H. B. Pei, and Z. Y. Chan, "Numerical simulation on crack propagation of coal bed deep-hole cumulative blasting," *Mtan Xuebao/Journal of the China Coal Society*, vol. 37, no. 2, pp. 274–278, 2012.

[12] W. X. Gao and D. Lei, "Numerical simulation of deep-hole controlled cutting blasting and its practice," *IEEE.*vol. 30, no. 2, pp. 1–4, 2010.

[13] B. P. Sun, W. X. Gao, and S. S. Zhou, "Study on numerical simulation and application of blasting of tunnel excavation," *Beijing Ligong Daxue Xuebao/Transaction of Beijing Institute of Technology*, vol. 38, no. 10, pp. 1025–1029 and 1036, 2018.

[14] D. M. Guo, K. Liu, R. S. Yang, and Y. Li, "Simulation experiments on the mechanism of adjacent tunnel crack extension induced by explosion load," *Journal of Vibration and Shock*, vol. 35, no. 2, pp. 178–183, 2016.

[15] K. Gunaryo, H. Heriana, M. R. Sitompul, A. Kuswoyo, and B. K. Hadi, "Experimentation and numerical modeling on the response of woven glass/epoxy composite plate under blast impact loading," *International Journal of Mechanical and Materials Engineering*, vol. 15, no. 1, pp. 1–9, 2020.

[16] X. Wu, X. Li, S. Zhang, and K. Li, "Model experiment study on the effect of casting parameters on the cast percentage of high bench cast blasting," *Journal of Underground Space and Engineering*, vol. 15, no. 6, pp. 1889–1894+1902, 2019.

[17] L. I. Yao, L. I. He-Ping, and W. U. Xu-Tao, "Research on the HJC dynamic constitutive model for concrete," *Journal of Hefei University of Technology(Natural Science)*, vol. 32, no. 8, pp. 1244–1248, 2009.

[18] S. Wu, J. H. Zhao, J. Wang, N. Li, and Y. Li, "Study on parameters of HJC constitutive model based on numerical simulation of concrete SHPB test," *Chinese Journal of Computational Mechanics*, vol. 32, no. 6, pp. 789–795, 2015.

[19] Y. Zhang, F. Hu Hao, Q Zheng et al., "Calculation method for medium penetration coefficient of high-performance concrete," *Protective Engineering*, vol. 43, no. 2, pp. 31–38, 2021.

[20] G. Ren, W. U. Hao, Q. Fang, J. Zhou, and Z. Gong, "Determinations of HJC constitutive model parameters for normal strength concrete," *Journal of Vibration and Shock*, vol. 35, no. 18, pp. 9–16, 2016.

[21] Y.-g. Zhang, J. Tang, Z.-y. He, J. Tan, and C. Li, "A novel displacement prediction method using gated recurrent unit model with time series analysis in the Erdaohe landslide," *Natural Hazards*, vol. 105, no. 1, pp. 783–813, 2021.

[22] Y. Zhang and L. Yang, "A novel dynamic predictive method of water inrush from coal floor based on gated recurrent unit model," *Natural Hazards*, vol. 105, no. 2, pp. 2027–2043, 2021.

[23] C. Mark, "An updated empirical model for ground control in U.S. multiseam coal mines," *International Journal of Mining Science and Technology*, vol. 31, no. 2, pp. 163–174, 2021.

[24] Y.-g. Zhang, J. Tang, R.-p. Liao et al., "Application of an enhanced BP neural network model with water cycle algorithm on landslide prediction," *Stochastic Environmental Research and Risk Assessment*, vol. 35, no. 6, pp. 1273–1291, 2021.

[25] H. Rafezi and F. Hassani, "Drilling signals analysis for tricone bit condition monitoring," *International Journal of Mining Science and Technology*, vol. 31, no. 2, pp. 187–195, 2021.

[26] L. Qiu, Z. Liu, E. Wang, X. He, J. Feng, and B. Li, "Early-warning of rock burst in coal mine by low-frequency electromagnetic radiation," *Engineering Geology*, vol. 279, no. 1, Article ID 105755, 2020.

[27] Q. Ma, Y. Tan, X. Liu, Q. Gu, and X. Li, "Effect of coal thicknesses on energy evolution characteristics of roof rock-coal-floor rock sandwich composite structure and its damage constitutive model," *Composites Part B: Engineering*, vol. 198, no. 1, Article ID 108086, 2020.

[28] W. Hou, H. Wang, L. Yuan, W. Wang, Y. Xue, and Z. Ma, "Experimental research into the effect of gas pressure, particle size and nozzle area on initial gas-release energy during gas desorption," *International Journal of Mining Science and Technology*, vol. 31, no. 2, pp. 253–263, 2021.

[29] X. Liu, D. Fan, Y. Tan et al., "Failure evolution and instability mechanism of surrounding rock for close-distance parallel chambers with super-large section in deep coal mines," *International Journal of Geomechanics*, vol. 21, no. 5, Article ID 04021049, 2021.

[30] X. Liu, D. Fan, Y. Tan et al., "New detecting method on the connecting fractured zone above the coal face and a case study," *Rock Mechanics and Rock Engineering*, vol. 54, pp. 1–13, 2021.

[31] D.-y. Fan, X.-s. Liu, Y.-l. Tan, S.-l. Song, J.-g. Ning, and Q. Ma, "Numerical simulation research on response characteristics of

surrounding rock for deep super-large section chamber under dynamic and static combined loading condition," *Journal of Central South University*, vol. 27, no. 12, pp. 3544–3566, 2020.

[32] L. Qiu, D. Song, Z. Li, B. Liu, and J. Liu, "Research on AE and EMR response law of the driving face passing through the fault," *Safety Science*, vol. 117, pp. 184–193, 2019.

[33] X. Liu, S. Song, Y. Tan et al., "Similar simulation study on the deformation and failure of surrounding rock of a large section chamber group under dynamic loading," *International Journal of Mining Science and Technology*, vol. 31, no. 3, pp. 495–505, 2021.

[34] Y. Zhang, J. Qiu, Y. Zhang, and Y. Xie, "The adoption of a support vector machine optimized by GWO to the prediction of soil liquefaction," *Environmental Earth Sciences*, vol. 80, no. 9, p. 360, 2021.

[35] Y. Zhang, Y. Xie, Y. Zhang, J. Qiu, and S. Wu, "The adoption of deep neural network (DNN) to the prediction of soil liquefaction based on shear wave velocity," *Bulletin of Engineering Geology and the Environment*, vol. 80, no. 6, pp. 5053–5060, 2021.

[36] Y.-g. Zhang, J. Qiu, Y. Zhang, and Y. Wei, "The adoption of ELM to the prediction of soil liquefaction based on CPT," *Natural Hazards*, vol. 107, no. 1, pp. 539–549, 2021.

[37] W. Tang, C. Zhai, J. Xu, Y. Sun, Y. Cong, and Y. Zheng, "The influence of borehole arrangement of soundless cracking demolition agents (SCDAs) on weakening the hard rock," *International Journal of Mining Science and Technology*, vol. 31, no. 2, pp. 197–207, 2021.

[38] J. Wang, J. Yang, F. Wu, T. Hu, and S. A. Faisal, "Analysis of fracture mechanism for surrounding rock hole based on water-filled blasting," *International Journal of Coal Science & Technology*, vol. 7, no. 4, 2020.

[39] P. V. Nikolenko, S. A. Epshtein, V. L. Shkuratnik, and P. S. Anufrenkova, "Experimental study of coal fracture dynamics under the influence of cyclic freezing-thawing using shear elastic waves," *International Journal of Coal Science & Technology*, vol. 8, pp. 562–574, 2021.

[40] H. Xianjie, W. Hao, Y. Du et al., "Dynamic tensile behaviour and crack propagation of coal under coupled static-dynamic loading," *International Journal of Mining Science and Technology*, vol. 30, no. 5, pp. 659–668, 2020.